Asymmetric Drainage in Foam Films

ARTICLE *in* MRS ONLINE PROCEEDING LIBRARY · SEPTEMBER 1994

DOI: 10.1021/la00021a046

3 AUTHORS, INCLUDING:

G. J. Hirasaki
Rice University
178 PUBLICATIONS **3,331** CITATIONS
SEE PROFILE

Clarence A. Miller
Rice University
141 PUBLICATIONS **3,423** CITATIONS
SEE PROFILE

Asymmetric Drainage in Foam Films

Jean-Luc Joye, George J. Hirasaki, and Clarence A. Miller*

Department of Chemical Engineering, Rice University, P.O. Box 1892, Houston, Texas 77251

Received December 13, 1993. In Final Form: April 4, 1994®

The same basic mechanism is responsible for asymmetric drainage of thin circular films and marginal regeneration in vertical, rectangular films. A linear stability analysis showed that these phenomena are caused by a hydrodynamic instability that is produced by a surface-tension-driven flow and stabilized by surface viscosity, surface diffusivity, and the system length scale. A criterion for the onset of this instability was derived. Experiments performed on small circular films of aqueous solutions of SDS and SDS–1-dodecanol demonstrated the strong stabilizing effect of surface viscosity. Experimental results were found to be in good agreement with the predictions of the linear stability analysis.

Introduction

Drainage of thin liquid films is important for processes involving emulsions or foams. Most of the work done on modeling drainage of small circular films has been limited to the case of axisymmetric flow.[1–9] Experimental studies indicate that drainage is frequently asymmetric.[10,11] The reasons for this behavior are not well understood. However, it is known that asymmetric drainage is associated with mobile films, greatly increases the rate of film drainage, and can thus influence the rate of foam or emulsion coalescence.

Mysels et al.[10] were the first to investigate in detail the different types of thin film drainage, concentrating on vertical films formed by withdrawal of glass frames from pools of surfactant solutions. They observed mobile films which drained in minutes and showed turbulent motions along the edges and rigid films which drained in hours and showed little or no motion. They proposed that the rapid drainage and turbulence seen for the mobile films were the result of "marginal regeneration", a phenomenon in which thick film flowed into the Plateau borders near the legs of the frame at some elevations owing to the greater suction force exerted on thick films by the low pressure in the borders. Simultaneously, a thin film was pulled out of the borders at other elevations to maintain constant surface area for the overall film. Prins and van Voorst Vader[12] and Lucassen[13] showed that marginal regeneration caused by this mechanism would be suppressed in systems having a high surface dilational modulus. Hudales and Stein[14,15] observed marginal regeneration in mobile, vertical films and made measurements of film thickness as a function of position and time. Baets and Stein[16] described experimental observations of a phenomenon similar to marginal regeneration that developed at the base of their vertical films. On the basis of these observations Stein[17,18] proposed a modified mechanism for marginal regeneration which, in essence, attributed it to a hydrodynamic instability. However, no quantitative stability analysis was given.

We argue below that asymmetric drainage in circular films, marginal regeneration, and the behavior observed by Baets and Stein[13] in vertical films all stem from the hydrodynamic instability described in general terms by Stein.[17,18] After describing experimental results which demonstrate that high values of surface shear viscosity can prevent asymmetric drainage, we develop a linear stability analysis which provides a criterion for the transition from asymmetric to symmetric film drainage or for the occurrence of marginal regeneration in terms of film dimensions and surfactant properties.

Experimental Results

Experiments on drainage of horizontal, circular films were conducted using the interference method proposed by Deryagin[19] and Scheludko and Exerowa.[20] The details of the experimental approach and procedure have been reported in ref 9.

Experiments were performed on aqueous foam film drainage with different surfactant systems, such as sodium dodecyl sulfate (SDS), sodium dodecylbenzenesulfonate (SDBS), saponin (a plant derivative), α–olefinsulfonate (AOS) 14–16, 16–18, 18, and 20–24, internal olefinsulfonate (IOS) 15–17, and Chevron Chaser SD1000. Two different types of drainage were observed, symmetric and asymmetric. During symmetric film drainage, the interference patterns, recorded on video tape, were symmetric during the entire film drainage. Numerical simulation of symmetric drainage was carried out earlier by Joye et al.,[9] who also presented some experimental results. In contrast to this behavior, Figure 1 shows asymmetric drainage of a foam film containing 0.2 wt % SDBS. Initially, the drainage is symmetric and a dimple forms (Figure 1a). However, about 1/2 s later, interference patterns are no longer symmetric (Figure 1b), and asymmetric drainage takes place. Fluctuations in film

* To whom correspondence should be addressed.

® Abstract published in *Advance ACS Abstracts,* August 1, 1994.

(1) Reynolds, O. *Philos. Trans. R. Soc. London* **1886,** *177,* 157.
(2) Malhotra, A. K.; Wasan, D. T. *AIChE J.* **1987,** *33* (9), 1533–1541.
(3) Ruckenstein, E.; Sharma, A. *J. Colloid Interface Sci.* **1987,** *119* (1), 1–13.
(4) Barber, A. D.; Hartland, S. *Can. J. Chem. Eng.* **1976,** *54,* 279.
(5) Hartland, S. *Chem. Eng. Prog. Symp. Ser.* **1969,** *65,* 82.
(6) Frankel, S. P.; Mysels, K. J. *J. Phys. Chem.* **1964,** *66,* 190.
(7) Jain, R. K.; Ivanov, I. B. *J. Chem. Soc., Faraday Trans. 2* **1980,** *76,* 250.
(8) Lin, C.-Y.; Slattery, J. C. *AIChE J.* **1982,** *28,* 787.
(9) Joye, J.-L.; Hirasaki, G. J.; Miller, C. A. *Langmuir* **1992,** *8* (12), 3085–3092.
(10) Mysels, K. J.; Shinoda, K.; Frankel, S. *Soap Films* **1959.**
(11) Burrill, K. A.; Woods, D. R. *J. Colloid Interface Sci.* **1973,** *42,* 151.
(12) Prins, A.; van Voorst Vader, F. *Proc. 6th Int. Congr. Surf. Act. Subst. (Zurich)* **1972,** 441.
(13) Lucassen, J. In *Anionic Surfactants: Physical Chemistry of Surfactant Action*; Lucassen-Reynders, E. H., Ed.; Dekker: New York, 1981; pp 11, 255.
(14) Hudales, J. B.; Stein, H. N. *J. Colloid Interface Sci.* **1990,** *137,* 512–526.
(15) Hudales, J. B.; Stein, H. N. *J. Colloid Interface Sci.* **1990,** *138,* 354–364.
(16) Baets, P. J. M.; Stein, H. N. *Langmuir* **1992,** *8,* 3099–3101.
(17) Stein, H. N. *Adv. Colloid Interface Sci.* **1991,** *34,* 175–190.
(18) Stein, H. N. *Colloids Surf. A: Physicochem. Eng. Aspect* **1993,** *79,* 71–80.
(19) Deryagin, B. V.; Tilievskaya, A. S. *Proc. Second Int. Congr. Surf. Act.* **1957,** *1,* 211.
(20) Scheludko, A.; Exerowa, D. *Kolloid-Z.* **1957,** *155,* 39.

0743-7463/94/2410-3174$04.50/0

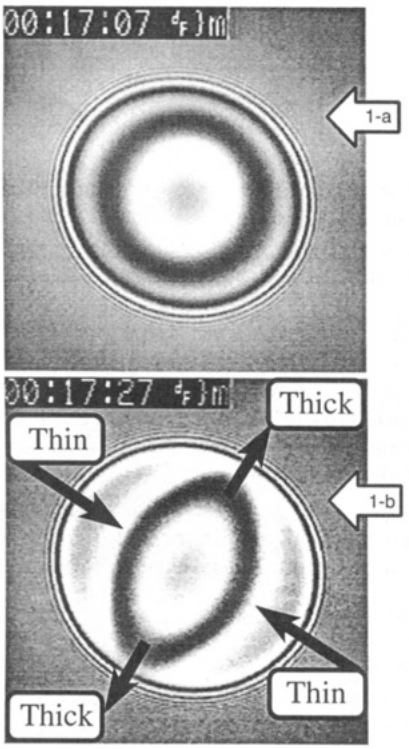

Figure 1. Drainage of SDBS (0.2 wt %). Film radius = 100 μm. Film drainage started at 00:15:00. A typical case of asymmetric drainage.

thickness around the barrier ring cause liquid in the thick parts of the film to flow more rapidly from the dimple into the meniscus region while thin parts get thinner and extend further into the film. The dimple is squeezed, deforms, and eventually slips to one side into the meniscus. Asymmetric drainage was found to always be much faster than symmetric drainage.

Films of most surfactant solutions were found to drain asymmetrically and very fast; exceptions were solutions of saponin and AOS 16−18. By adding a small quantity of 1-dodecanol to solutions of SDS, drainage became symmetric and much slower. A ratio of 1 molecule of 1-dodecanol to 100 molecules of SDS was used. Previous work[21] showed that the addition of 1-dodecanol to aqueous solutions of SDS greatly increased the surface shear viscosity. At low surfactant concentration, where the surface concentrations of surfactant and alcohol were low, causing a low surface shear viscosity, we observed asymmetric drainage. Near the critical micelle concentration (CMC), where the surface concentrations of surfactant and alcohol were high, causing a high surface shear viscosity, we observed symmetric drainage. Well above the CMC, most of the alcohol was solubilized by the micelles in solution. As a result the surface concentration of alcohol was lowered, causing a decrease in surface viscosity and a return to asymmetric drainage.

Figure 2 shows the drainage time of SDS and SDS−1-dodecanol (100:1) films as a function of surface shear viscosity. Similar results were obtained by adding 1-dodecanol to solutions of AOS 14-16. The transition from asymmetric to symmetric drainage was found to be strongly dependent on the value of surface shear viscosity. Symmetric drainage was associated with rigid surfaces that permit little or no tangential flow, as indicated by high values of surface shear viscosity. Asymmetric drainage was associated with more mobile and deformable

(21) Djabbarah, N. F.; Shah, D. O.; Wasan, D. T. *Colloid Polym. Sci.* **1978**, *256*, 1002−1008.

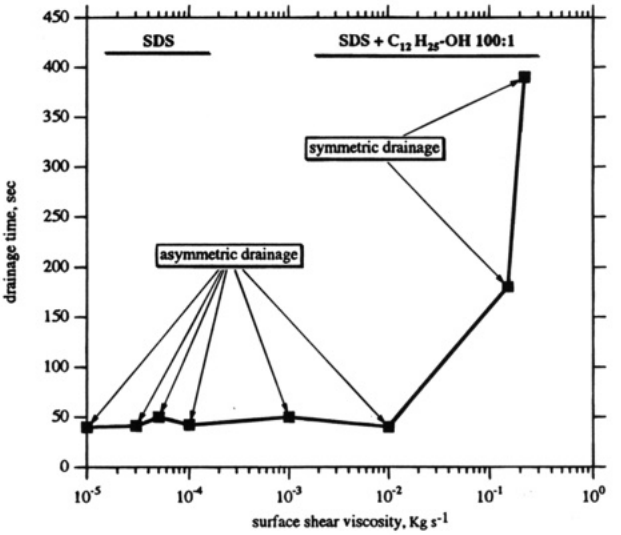

Figure 2. Drainage time as a function of surface shear viscosity for SDS and SDS−$C_{12}H_{25}OH$ (100:1). Film radius ≈ 100 μm. Surface shear viscosity from Djabbarah.[21]

surfaces which have low surface shear viscosity. As discussed in the following section, other parameters such as surface dilational viscosity, surface diffusivity, and system size are also factors in determining the drainage type.

Linear Stability Analysis

In the case of horizontal film drainage, we approximate the film region between the dimple and meniscus (barrier ring) by a film initially of uniform half-thickness h_0 (see Figure 3). For simplicity we use Cartesian coordinates instead of cylindrical coordinates in this analysis to clarify the basic mechanism of instability as shown in Figure 3b. This assumption is reasonable when the width in the direction of flow of the barrier ring is small compared to the circumference of the barrier ring. For a typical film radius R_f of 100 μm, numerical solutions (see Joye et al.[9]) show that the width of the barrier ring is around 25 μm and is much smaller than the circumference of the ring $2\pi R_f$ which is 628 μm. During film drainage most of the pressure gradient takes place in the barrier ring region. The pressure gradient, causing the underlying bulk liquid to flow from the dimple into the meniscus, is assumed to be constant. We assume that the interface contains an insoluble monolayer of surfactant which, at rest, has a uniform surface concentration Γ_{eq}.

Steady-State Solution. We consider the steady-state solution with uniform thickness h_0 and immobile interface, $v_s^{ss} = 0$. The average x and y components of velocity of the underlying bulk liquid are given by

$$\bar{v}_x^{ss} = -\frac{h_0^2}{3\mu}\left(\frac{\partial P^{ss}}{\partial x}\right) \tag{1}$$

and

$$\bar{v}_y^{ss} = 0 \tag{2}$$

The underlying liquid generates a constant tangential stress at the interface that must be balanced by a constant surface tension gradient in order to have an immobile interface. Therefore, we have

$$\left(\frac{\partial \sigma^{ss}}{\partial x}\right) = -\mu \left.\frac{\partial v_x^{ss}}{\partial z}\right|_{z=h_0} = h_0\left(\frac{\partial P^{ss}}{\partial x}\right) \tag{3}$$

The surface tension σ can be related to the surface

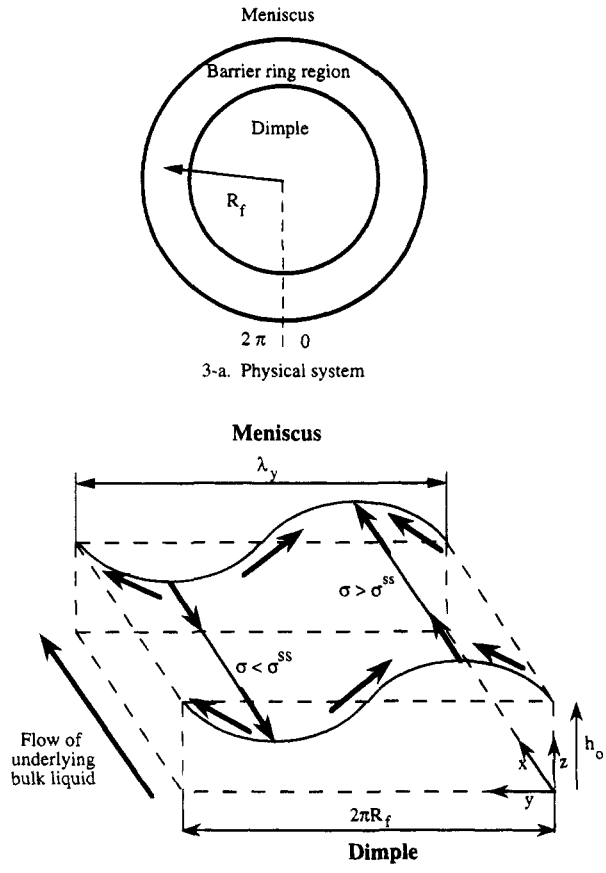

Figure 3. Schematic view of perturbations in thickness, surface velocity, and surface tension in an unstable film.

concentration of surfactant Γ by an equation of state: $\sigma = -\alpha\Gamma + C$, where $\alpha = -(\partial\sigma/\partial\Gamma)_{eq}$ and C is a constant. Hence, eq 3 can be written as

$$\left(\frac{\partial\Gamma^{ss}}{\partial x}\right) = -\frac{h_0}{\alpha}\left(\frac{\partial P^{ss}}{\partial x}\right) \tag{4}$$

The tangential stress induces a constant surfactant concentration gradient, given by eq 4, in the same direction as the underlying liquid flow.

We realize that the pressure gradient in the direction of flow generates a curvature gradient in this direction. These curvature effects are neglected in the above steady-state solution and in the following linear stability analysis. It is assumed that the wavelengths associated with the perturbations introduced below are much smaller than the minimum radius of curvature before perturbation in the xz plane of Figure 3b. A numerical model which includes variation in thickness in the direction of flow has been developed to simulate the instability causing asymmetric drainage. The results show that deviations from predictions of the linear stability analysis are very small when this condition is satisfied.[22] Detailed information on the simulations will be published separately.

Stability Analysis. The stability of the steady-state solution is investigated by considering a small spatial and temporal perturbation for each of the dependent variables around the steady state:

$$\tilde{h} = h - h_0 \tag{5}$$

$$\tilde{\Gamma} = \Gamma - \Gamma^{ss} \tag{6}$$

(22) Joye, J.-L. Mechanisms of Symmetric and Asymmetric drainage in Foam Films. Ph.D. Thesis, Rice University, 1994.

$$\tilde{v}_{sx} = v_{sx} - 0 \tag{7}$$

$$\tilde{v}_{sy} = v_{sy} - 0 \tag{8}$$

$\tilde{v}_{sx}$ and $\tilde{v}_{sy}$ are, respectively, the x and y components of the surface velocity.

For simplicity, we assume that perturbations are independent of x. Consequently, no boundary conditions are specified in the direction of flow, and perturbations in this direction are not considered. Accordingly, the following analysis is limited to the case where the wavelength of an unstable perturbation in the transverse direction is small compared to the minimum radius of curvature of the barrier ring, the same assumption as discussed previously. Unstable perturbations satisfying this condition exist at least when the surface viscosity is low as demonstrated below.

Neglecting second-order terms, the equations of change for the perturbations are linearized. In the lubrication approximation, the equations are as follows:

Bulk liquid mass balance:[23]

$$\frac{\partial\tilde{h}}{\partial t} = -h_0\frac{\partial}{\partial y}(\tilde{v}_{sy}) - \frac{\sigma h_0^3}{3\mu}\left(\frac{\partial^4\tilde{h}}{\partial y^4}\right) \tag{9}$$

Surfactant mass balance:[24] We assume that the surfactant concentration gradient necessary to balance the shear stress at the surface is very small compared to the uniform concentration of surfactant present in the absence of flow ($\Gamma^{ss} \approx \Gamma_{eq}$). Calculations show that this is the case for situations of interest. The surfactant mass balance becomes

$$\frac{\partial\tilde{\Gamma}}{\partial t} = -\left(\frac{\partial\Gamma^{ss}}{\partial x}\right)\tilde{v}_{sx} - \Gamma_{eq}\frac{\partial\tilde{v}_{sy}}{\partial y} + D_s\frac{\partial^2\tilde{\Gamma}}{\partial y^2} \tag{10}$$

D_s is the surface diffusivity.

Surface momentum equations (inertial effects are neglected):[24]

x component

$$\mu_s\frac{\partial^2\tilde{v}_{sx}}{\partial y^2} = \tilde{h}\left(\frac{\partial P^{ss}}{\partial x}\right) \tag{11}$$

y component

$$-\alpha\frac{\partial\tilde{\Gamma}}{\partial y} + (\mu_d + \mu_s)\frac{\partial^2\tilde{v}_{sy}}{\partial y^2} = -\sigma h_0\left(\frac{\partial^3\tilde{h}}{\partial y^3}\right) \tag{12}$$

where μ_d and μ_s are, respectively, the surface dilational and shear viscosities.

Consider the following perturbations:

$$\tilde{h} = \hat{h}\exp(\beta t + ik_y y) \tag{13}$$

$$\tilde{\Gamma} = \hat{\Gamma}\exp(\beta t + ik_y y) \tag{14}$$

$$\tilde{v}_{sx} = \hat{v}_{sx}\exp(\beta t + ik_y y) \tag{15}$$

(23) Ivanov, I. B. *Thin Liquid Films*; Marcel Dekker: New York, 1988; Chapter 11.

(24) Edwards, D. A.; Brenner, H.; Wasan, D. T. *Interfacial Transport Processes and Rheology*; Butterworth-Heinemann Series in Chemical Engineering; Butterworth-Heinemann: London, 1991; Chaper 16, 436–437.

$$\tilde{v}_{sy} = \hat{v}_{sy} \exp(\beta t + ik_y y) \tag{16}$$

where $\hat{h}$, $\hat{\Gamma}$, $\hat{v}_{sx}$, and $\hat{v}_{sy}$ are constants, k_y is the wavenumber in the y direction, and β is the growth factor. k_y is equal to $2\pi/\lambda_y$ where λ_y is the wavelength of the perturbations as shown in Figure 3. Substitution of the above expressions for the perturbations $\tilde{h}$, $\tilde{\Gamma}$, $\tilde{v}_{sx}$, and $\tilde{v}_{sy}$ into the differential equations and definition of the following dimensionless variables

$$W = \frac{\Gamma\alpha}{3\mu\bar{v}_x^{ss}}, \quad H = \frac{h}{h_0}, \quad U = \frac{v_{sx}}{3\bar{v}_x^{ss}} S_{sh}$$

$$V = \frac{v_{sy}}{3\bar{v}_x^{ss}} S_{sh}, \quad \beta' = \beta\left(\frac{\mu_s}{3\mu\bar{v}_x^{ss}}\right), \quad K = h_0 k_y$$

yield the following set of equations:

$$\beta'\hat{H} = -iK\hat{V} - \left(\frac{S_{sh}}{9Ca}\right)K^4\hat{H} \tag{17}$$

$$\beta'\hat{W} = -\hat{U} - iK\left(\frac{E_d}{3Ca}\right)\hat{V} - \frac{K^2}{Ma}\hat{W} \tag{18}$$

$$K^2\hat{U} = \hat{H} \tag{19}$$

$$-iK\hat{W} - \left(\frac{S_{d+sh}}{S_{sh}}\right)K^2\hat{V} = i\frac{K^3}{3Ca}\hat{H} \tag{20}$$

In order to have a nontrivial solution for $\hat{H}$, $\hat{W}$, $\hat{U}$, and $\hat{V}$, the determinant of the above set of equations must be equal to zero. This yields a second-order polynomial in β' with real coefficients. β' was found to be real and given by the following expression:

$$\beta' = \frac{-(a+c) + [(a-c)^2 + 4bd]^{1/2}}{2} \tag{21}$$

with

$$a = \frac{S_{sh}K^2}{3S_{sh+d}Ca}\left(1 + \frac{S_{sh+d}}{3}K^2\right) \quad b = \frac{1}{K^2} + \frac{E_d S_{sh}}{9S_{sh+d}Ca^2}K^2$$

$$c = \frac{E_d S_{sh}}{3S_{sh+d}Ca}\frac{K^2}{Ma} \quad d = \frac{S_{sh}}{S_{sh+d}}$$

The sign of β' is given by

$$\frac{K^6}{3(Ma)(Ca)}\left(1 + \frac{(Ma)S_{sh}}{3Ca}\frac{E_d}{3} + \frac{S_{sh+d}K^2}{3}\right)$$

$$\begin{cases} >1, \beta' < 0, \text{ stable system} \\ =1, \beta' = 0, \text{ marginal stability} \\ <1, \beta' > 0, \text{ unstable system} \end{cases} \tag{22}$$

with

$$Ca = \frac{\mu\bar{v}_x^{ss}}{\sigma}, \quad E_d = \frac{\Gamma_{eq}\alpha}{\sigma}, \quad S_{sh} = \frac{\mu_s}{\mu h_0}$$

$$S_{d+sh} = \frac{\mu_d + \mu_s}{\mu h_0}, \quad Ma = \frac{\alpha(\partial\Gamma^{ss}/\partial x)h_0^3}{D_s\mu_s}$$

If β' is positive, small perturbations grow and the system is unstable. If β' is negative, small perturbations are damped and the system is stable. Ca is a capillary number, Ma is a surface Marangoni number, E_d is a dimensionless elasticity, and S_{sh} and S_{d+sh} are dimensionless surface viscosity groups. Scriven and Sternling[25] defined a "crispation number" in their analysis of Marangoni instability in a thin layer heated from below. A similar crispation number, Cr, can be defined for the present system and is expressed as follows:

$$Cr = \frac{3Ca}{(Ma)S_{sh}} = \left(\frac{\mu D_s}{h_0\sigma}\right)$$

Expression 22 becomes

$$\frac{K^6}{3(Ma)(Ca)}\left(1 + \frac{E_d}{3Cr} + \frac{S_{sh+d}K^2}{3}\right)$$

$$\begin{cases} >1, \beta' < 0, \text{ stable system} \\ =1, \beta' = 0, \text{ marginal stability} \\ <1, \beta' > 0, \text{ unstable system} \end{cases} \tag{23}$$

It is clear that large capillary, Marangoni, and crispation numbers promote instability whereas large surface elasticity, large shear and dilational viscosity, and a large wavenumber promote stability.

Substitution of expressions for the dimensionless parameters Ca, E_d, Ma, S_{d+sh}, S_{sh}, and K in expression 22 yields the following stability criterion:

$$\left(\frac{D_s\mu_s\sigma}{(-\partial P^{ss}/\partial x)^2} + \frac{\sigma h_o\mu_s\Gamma_{eq}\alpha}{3\mu(-\partial P^{ss}/\partial x)^2}\right)\left(\frac{2\pi}{\lambda_y}\right)^6 + \left(\frac{\sigma D_s\mu_s(\mu_d + \mu_s)h_o}{3\mu(-\partial P^{ss}/\partial x)^2}\right)\left(\frac{2\pi}{\lambda_y}\right)^8 \begin{cases} >1, \text{ stable} \\ =1, \text{ marginal} \\ <1, \text{ unstable} \end{cases} \tag{24}$$

We expressed the average bulk velocity and surface concentration gradient as a function of the pressure gradient in this equation because the latter can be approximated by the difference between the pressure in the meniscus and pressure in the dimple divided by the length of the barrier ring region. These quantities can be obtained from experiments on film drainage.

Note that in the linear stability analysis described above, the decrease in thickness over time due to film drainage is neglected. As indicated by Frankel–Mysels theory[26] and our simulations,[9] drainage at the barrier ring for the case of large dimples and immobile interfaces can be described by Reynolds' theory. In the case of a typical film drainage experiment (parameters are given in Table 1), the rate of decrease in thickness due to film drainage at the barrier ring can be estimated using Reynolds' formula. A 10% decrease takes around 2 s at a thickness of 200 nm. Table 1 shows the reciprocal of β at different SDS and SDS–1-dodecanol concentrations for the same conditions. For pure SDS (low surface shear viscosity) β^{-1}, the characteristic time for instability to develop, is no greater than about 0.25 s and hence much smaller than the time it takes for the film to thin by 10%. Therefore, the assumption of neglecting the change in thickness due to film drainage is valid, at least for low surface shear viscosity.

Discussion

The linear stability analysis shows that the mechanism of asymmetric drainage is a surface-tension-driven instability that is stabilized by surface viscosity, surface diffusivity, surface elasticity, and the system length scale. Consider a periodic perturbation in thickness as shown in Figure 3. In the thick parts of the film, the shear stress

(25) Scriven, L. E.; Sternling, C. V. *J. Fluid Mech.* **1964**, *19*, 321–340.
(26) Frankel, S. P.; Mysels, K. J. *J. Phys. Chem.* **1962**, *66*, 190.

Table 1. Comparison of Experimental Results for SDS and SDS−1-Dodecanol (100:1) with Linear Stability Analysis[a]

concn (kg m^{-3})	μ_s (kg s^{-1})	$\mu_d + \mu_s$ (kg s^{-1})	$\Gamma_{eq}\alpha$ (N m^{-1})	left side of eq 24	experimental drainage observation	$1/\beta$ (s)
			Pure SDS			
0.2	3×10^{-8}	10^{-4}	5×10^{-3}	5×10^{-6}	asymmetric	1.7×10^{-2}
0.6	5×10^{-8}	1.6×10^{-3}	0.011	3×10^{-4}	asymmetric	0.1
1.2	10^{-7}	2×10^{-3}	0.024	1.6×10^{-3}	asymmetric	0.25
3.5	10^{-8}	1.6×10^{-3}	0.014	7.6×10^{-5}	asymmetric	4×10^{-2}
			SDS−1-Dodecanol (100:1)			
0.2	10^{-5}	2×10^{-4}	0.01	0.887	asymmetric	7
0.6	1.5×10^{-4}	1.5×10^{-2}	0.016	31	symmetric	$\beta < 0$
1.2	2.1×10^{-4}	4×10^{-2}	0.021	75	symmetric	$\beta < 0$
3.5	10^{-6}	2.5×10^{-2}	5×10^{-3}	0.05	asymmetric	1.2

[a] $\sigma = 3.3 \times 10^{-2}$ N m^{-1}, $P_c = 35$ Pa, $P_d = 0$, $D_s = 5 \times 10^{-9}$ m^2 s^{-1}, $R = 100$ μm, $\lambda_y = 2\pi R$, $h_0 = 100$ nm, $\mu = 10^{-3}$ kg m^{-1} s^{-1}. If the left side of eq 24 is less than 1, instability occurs, and if greater than 1, the system is stable. Data obtained from Djabbarah.[21,27]

at the surface due to the flow of the underlying liquid is larger than the initial surface tension gradient. Hence, surface flow is established in the same direction as the flow of the underlying liquid (from the dimple to the meniscus) that results in a decrease in surfactant concentration and an increase in surface tension in the film. In the thin parts of the film the shear stress at the surface is lower than the initial surface tension gradient, causing surface flow in the reverse direction (from the meniscus to the dimple). The surfactant concentration increases and the surface tension decreases in the film. Therefore, in the direction perpendicular to the initial flow (y direction), surface tension gradients cause the surface and underlying fluid to flow from thin to thick parts of the film. As a result, perturbations grow and the system is unstable. For sufficiently small wavelengths, capillary flows (curvature driven), which promote flow in the direction opposite to the surface-tension-driven flow, can prevent the instability from occurring. Surface diffusivity decreases surface tension gradients and therefore dampens the effect of surface-tension-driven flow. Surface shear viscosity and dilational viscosity are also stabilizing factors due to their energy dissipating effect. In the stability criterion,[24] one can see that every term is multiplied by surface shear viscosity μ_s. This property is therefore a key factor in determining the transition from symmetric drainage to asymmetric drainage as indicated by our experimental results.

Experiments on the radial film drainage of pure SDS and SDS−1-dodecanol can be compared with our linear stability analysis by taking the wavelength λ_y of the perturbation equal to $2\pi R$, the circumference of the film, and using Djabbarah's data[27] on surface dilational and shear viscosity and elasticity for these systems. This value of λ_y represents the longest possible wavelength and hence the least stable perturbation which can develop. Comparisons of the linear stability predictions with our experimental results are listed in Table 1. As one can see, asymmetric drainage is seen whenever the left side of criterion 24 is less than 1, in agreement with the theory.

The linear stability analysis can also be applied to marginal regeneration observed in the drainage of vertical films formed by withdrawal of glass frames. Two sites for marginal regeneration were observed.[18] The first one is located at the vertical film/Plateau border boundaries where liquid flows horizontally from the film into the border due to a pressure difference. In this case, the linear stability analysis applies and provides a quantitative description of the mechanism described above, which is basically that proposed by Stein.[17,18] It should be noticed that once this mechanism generates thick and thin regions, gravity may influence their motions within the film. But the instability is responsible for initial occurrence of significant variations in local thickness.

The second site for marginal regeneration is located at the film/bulk liquid transition,[16,18] where drainage is vertical and governed by gravity and the capillary suction in the transition region. Our stability analysis can also be applied to this situation by adding ϱg to $-\partial P^{ss}/\partial x$, where ϱ is the density of the bulk liquid and g the acceleration due to gravity. Stein[17,18] also observed that marginal regeneration never occurs at the film/Plateau border located at the top of the glass frame. A possible explanation of this observation is that gravity and capillary suction act in opposite directions, thereby reducing liquid flow in the film and shear stress at the surface.

A two-dimensional simulator was also developed[22] to simulate a section of a film in the transition or barrier ring region between the dimple and the meniscus where the thickness goes through a minimum. Assumptions were the same as those of the linear stability analysis except that variations in the x direction were permitted. First, a steady-state solution, with nonuniform film thickness in the x direction, was found for a specified pressure drop between the dimple and the meniscus. Then, the stability of the system was examined by imposing an initial perturbation in thickness around the steady-state solution in the direction transverse to the liquid flow. Although details of the simulations will be published separately, we found that their results confirmed the results of the above linear stability analysis when the shortest wavelength of an unstable perturbation in the transverse direction was small in comparison to the radius of curvature of the unperturbed film in the barrier ring region. It was found that this condition is satisfied for many conditions of interest, e.g., films of low surface shear viscosity. For example, for a typical film drainage experiment with pure SDS, the critical wavelength causing instability is around 100 μm and the minimum radius of curvature of the barrier ring is around 1 mm. However, departures from predictions of the linear analysis are observed when this condition is not satisfied.

Figure 4 shows a typical surface velocity plot as the instability develops. A circulation cell develops in the barrier ring region, causing thick parts of the film to thicken and the surface there to flow outward toward the meniscus, while thin parts of the film get thinner with the surface flowing inward toward the dimple, the same basic flow pattern as in the linear stability analysis. It should be mentioned that we used a symmetry condition at the transverse boundary in our simulations, which explains the development of a single circulation cell corresponding to half a wavelength of the linear stability analysis.

(27) Djabbarah, N. F. The Interrelationship Among Surface Composition, Surface Rheological Properties and Foam Stability. Ph.D. Thesis, Illinois Institute of Technology, 1978.

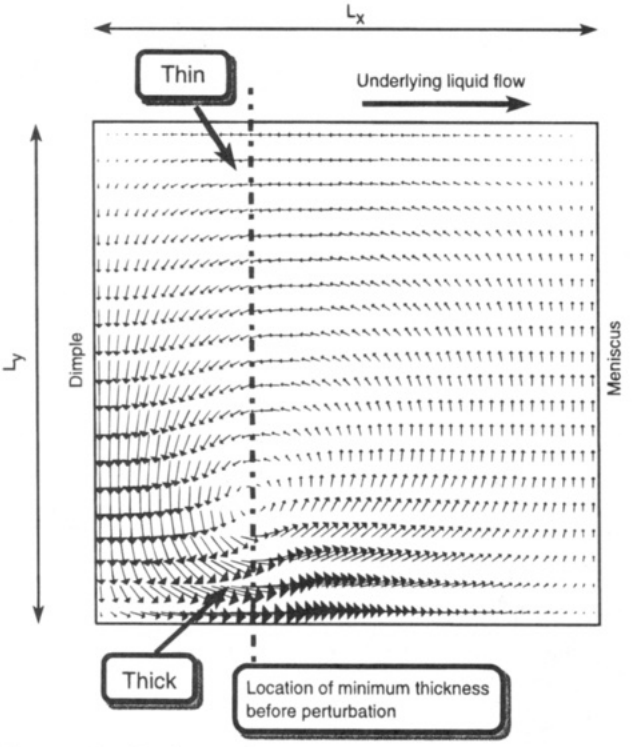

Figure 4. Surface velocity plot during instability from numerical simulation.

Conclusions

A criterion giving conditions for the onset of an instability causing asymmetric drainage in foam films was developed. Asymmetric drainage is the result of an instability involving surface-tension-driven flow that is stabilized by surface dilational viscosity, surface diffusivity, the system length scale, and especially surface shear viscosity. Predictions from the criterion are in good agreement with experimental observations. The criterion is also applicable to marginal regeneration in vertical films, which is produced by the same instability.

Acknowledgment. The present work was supported by the Texas Energy Research in Applications Program. The authors gratefully acknowledge A. D. Nikolov who provided us with one of his glass cells to perform the experiments and C. J. van Duijn for his help in the development of the linear stability analysis.

Notation

a = dimensionless group (eq 21)
b = dimensionless group (eq 21)
c = dimensionless group (eq 21)
C = constant, N m^{-1}
Ca = capillary number
Cr = crispation number
d = dimensionless group (eq 21)
D_s = surface diffusivity, m^2 s^{-1}
E_d = dimensionless elasticity
g = acceleration due to gravity, m s^{-2}
k_y = wavenumber in the y direction, m^{-1}
K = dimensionless k_y
h = half-thickness of the film, m
h_0 = uniform half-thickness solution of the steady-state solution, m
H = dimensionless half-thickness
Ma = Marangoni number
P = bulk pressure, Pa
P_c = capillary pressure, Pa
P_d = Pressure in the dimple, Pa
R = film radius, m
t = time, s
T = dimensionless time
v_s = surface velocity, m s^{-1}
U = dimensionless x component of surface velocity
V = dimensionless y component of surface velocity
v = bulk velocity, m s^{-1}
W = dimensionless concentration
S_{sh} = dimensionless surface shear viscosity group
S_{d+sh} = dimensionless surface dilational plus shear viscosity group

Greek Letters

α = concentration coefficient of interfacial tension, m^2 s^{-2}
β = time growth constant, s^{-1}
β' = dimensionless time growth constant
ϱ = density, kg m^{-3}
Γ = surfactant concentration at the surface, kg m^{-2}
Γ_{eq} = equilibrium surfactant concentration at the surface and at rest, kg m^{-2}
σ = interfacial tension, N m^{-1}
μ = bulk viscosity, kg m^{-1} s^{-1}
μ_s = surface shear viscosity, kg s^{-1}
μ_d = surface dilational viscosity, kg s^{-1}

Superscript

ss steady-state solution

Subscripts

x vector component in the x direction
y vector component in the y direction

Accents

$\bar{}$ average value
$\tilde{}$ perturbation around steady-state solution
$\hat{}$ amplitude of perturbations